Sensors and Materials, Vol. 37, No. 10 (2025) 4347–4364
MYU Tokyo

S & M 4186

Electrochemical Sensing of the Stimulant Ephedrine Using Conductive Polymer–Carbon Nanotube Composite Film-modified Electrodes

Ruiqing Dong,[1] Liuyang Li,[2*] Baosheng Pu,[3] and Nan Ding[4]

[1]Guangzhou College of Commerce, Physical Education Institute, GuangZhou 511363, China
[2]St. Paul University Philippines, Physical Education Institute, Tuguegarao, Cagayan 100600, Philippines
[3]Belarusian State University of Economics, Minsk 220070, Belarus
[4]Belarusian State University of Physical Education, Minsk 220020, Belarus

(Received July 1, 2025; accepted August 13, 2025)

Keywords: molecular imprinting, voltammetry, forensic analysis, drug monitoring, acrylamide

The escalating misuse of ephedrine in sports doping and illicit drug synthesis underscores the critical need for advanced detection platforms. In this paper, we describe in detail the development of a highly sensitive and selective electrochemical sensor for ephedrine, based on a molecularly imprinted polymer (MIP) integrated with conductive multiwalled carbon nanotubes (MWCNTs) and a conductive polymer layer onto a glassy carbon electrode. The fabrication involved functionalizing MWCNTs to enhance dispersibility, followed by the *in situ* polymerization of an ephedrine-imprinted acrylamide and *N*,*N*'-methylenebisacrylamide matrix. Extensive material characterization, including SEM and TEM, confirmed the formation of a porous, interconnected composite film with MWCNTs uniformly embedded within the MIP, featuring a polymer coating of approximately 10 nm, which is crucial for creating accessible molecular recognition sites. Electrochemical assessments via cyclic voltammetry (CV) and electrochemical impedance spectroscopy (EIS) verified significantly improved electron transfer kinetics and successful template imprinting, as evidenced by changes in redox behavior and charge transfer resistance. The sensor demonstrated exceptional analytical performance for ephedrine detection across a linear range of 0.05 to 50 μM, achieving an impressively low limit of detection (LOD) of 15 nM and a sensitivity of 26.03 μA/nM. It exhibited marked selectivity against structurally analogous interferents, notably pseudoephedrine (K = 5.6). The sensor's practical viability was robustly established with recovery rates between 95.4 and 103.5% in spiked human serum and urine. This MIP-CNT-based electrochemical sensor presents a significant advancement for rapid, cost-effective, and reliable ephedrine monitoring in clinical diagnostics and forensic science.

*Corresponding author: e-mail: mingsikeyangzong@163.com
https://doi.org/10.18494/SAM5834

ISSN 0914-4935

1. Introduction

The monitoring of stimulant drugs, particularly those with high abuse potential such as ephedrine, has become a pressing concern in the fields of public health, forensic science, and clinical diagnostics.[1] Ephedrine, a naturally occurring alkaloid[2] and synthetic stimulant,[3] is widely utilized for its bronchodilatory[4] and sympathomimetic effects.[5] However, its misuse in sports doping, illicit drug synthesis,[6] and unregulated weight loss regimens[2] has raised significant legal and health-related challenges. The accurate, rapid, and reliable detection of ephedrine in biological fluids and pharmaceutical preparations is therefore paramount for regulatory enforcement and clinical monitoring. Conventional analytical methods for detecting ephedrine, including high-performance liquid chromatography, gas chromatography-mass spectrometry, and capillary electrophoresis, have been the gold standard in laboratory settings. While these methods offer high sensitivity and specificity, they often require complex sample preparation, expensive instrumentation, and highly skilled personnel.[7] Additionally, their operational constraints render them unsuitable for on-site or point-of-care testing, where rapid decision-making is critical.[8] In this context, the development of portable, cost-effective, and highly selective sensing platforms is an urgent technological need.

Electrochemical sensors have emerged as promising alternatives to conventional analytical techniques owing to their inherent advantages, such as high sensitivity, low cost, ease of miniaturization, and compatibility with real-time and in-field monitoring.[9] These sensors translate chemical information into measurable electrical signals,[10] offering the quantitative detection of target analytes within complex matrices.[11] However, despite their significant promise, the practical deployment of electrochemical sensors for stimulant drug detection faces critical challenges, primarily associated with sensor selectivity and stability under physiological conditions. To overcome these limitations, the integration of molecularly imprinted polymers (MIPs) into electrochemical sensor designs has attracted substantial attention.[12,13] MIPs are synthetic polymers with highly specific recognition sites formed through a templating process involving the target molecule.[14] During polymerization, functional monomers interact with the target analyte, creating a complementary cavity that retains the memory of the analyte's size, shape, and functional groups after template removal.[15] These "artificial receptors" exhibit high selectivity and affinity toward the target molecule, even in the presence of structurally similar compounds.[16] Such molecular recognition capabilities position MIPs as ideal candidates for enhancing the selectivity of electrochemical sensors in complex environments such as biological fluids.[17]

Despite their advantageous properties, traditional MIP-based sensors often suffer from poor electrical conductivity and limited electron transfer efficiency, which restricts their sensitivity and responsiveness.[18] To address these shortcomings, recent advances in nanomaterials have opened new avenues for augmenting the performance of MIP-based electrochemical sensors.[19] Among these, carbon nanotubes (CNTs) have emerged as one of the most effective nanomaterials for electrode modification.[20,21] CNTs exhibit exceptional electrical conductivity,[22] high surface area,[23] chemical stability,[24] and mechanical strength,[25,26] making them ideal platforms for facilitating electron transfer processes and enhancing the sensitivity of electrochemical sensors.[27] When combined with MIPs, CNTs serve a dual purpose: they not

only improve the electrical conductivity of the sensing interface but also provide a high-surface-area scaffold for the uniform deposition of the imprinted polymer.[28,29] This hybridization significantly increases the density of recognition sites[30] and facilitates rapid electron transport, leading to improved signal-to-noise ratios and lower detection limits. Furthermore, the unique tubular structure of CNTs offers additional pathways for analyte diffusion, enhancing mass transport kinetics and reducing response time.

The design of conductive polymer-CNT composite films represents further refinement in the development of high-performance electrochemical sensors.[31] Conductive polymers such as polyaniline, polypyrrole, and polythiophene have been widely employed in sensor applications owing to their tunable electrical properties[32] and ease of functionalization.[33] These polymers can form strong interactions with both the CNT framework and the functional monomers used in molecular imprinting, resulting in robust composite materials with enhanced mechanical integrity and chemical stability. The synergistic effects of conductive polymers and CNTs not only facilitate effective signal transduction but also create a favorable microenvironment for the formation of highly selective molecular recognition sites. In the specific case of ephedrine detection, the application of MIP-CNT composite film-modified electrodes offers a strategic approach to overcome the challenges associated with low selectivity and the poor analytical performance of traditional sensors. By imprinting the sensor surface with ephedrine as the template molecule, the resulting cavities exhibit high binding affinity and selectivity toward ephedrine molecules, even in the presence of interfering compounds commonly found in biological fluids. The incorporation of CNTs further enhances the sensitivity and detection limit of the sensor, enabling the reliable quantification of ephedrine at trace levels.

In this study, we present the design, synthesis, and comprehensive evaluation of an electrochemical sensor based on a molecularly imprinted polymer-conductive polymer-carbon nanotube composite film for the highly sensitive and selective detection of ephedrine. The developed sensor leverages the molecular recognition capability of MIPs, the superior conductivity of CNTs, and the functional versatility of conductive polymers to achieve outstanding analytical performance. Extensive material characterization using Fourier-transform infrared spectroscopy (FTIR), X-ray diffraction (XRD), SEM, TEM, mapping analysis (MAP), and X-ray photoelectron spectroscopy (XPS) has been conducted to validate the structural integrity and functionalization of the composite materials. Electrochemical performance metrics, including sensitivity, selectivity, stability, repeatability, and real-sample applicability, are systematically explored.

2. Materials and Methods

2.1 Chemicals and reagents

Ephedrine hydrochloride (purity ≥ 99%) was obtained from Shanghai Aladdin Biochemical Technology Co., Ltd. Acrylamide (AAM), serving as the functional monomer, and *N*,*N*'-methylenebisacrylamide (MBA), employed as the cross-linking agent, were purchased from Sinopharm Chemical Reagent Co., Ltd. Ammonium persulfate (APS), used as the radical initiator, and sodium dodecyl sulfate (SDS), applied in the template removal process, were also

acquired from Sinopharm. Multiwalled carbon nanotubes (MWCNTs) with an outer diameter of 20–30 nm and a length of 10–15 μm, functionalized with carboxyl groups (–COOH), were purchased from Chengdu Organic Chemicals Co., Chinese Academy of Sciences. Conductive polymer polyaniline (emeraldine base, analytical grade) was supplied by Macklin Biochemical Co., Ltd.

Other supporting chemicals included glacial acetic acid, sodium chloride, potassium ferricyanide [$K_3Fe(CN)_6$], potassium ferrocyanide [$K_4Fe(CN)_6$], and phosphate-buffered saline (PBS), all procured from Tianjin Kemiou Chemical Reagent Co., Ltd. Ultrapure water with a resistivity of 18.2 MΩ·cm, produced by a Millipore Direct-Q water purification system, was used throughout the experiments.

2.2 Fabrication of MIP-CNT composite film-modified electrodes

MWCNTs were first functionalized to introduce carboxyl groups, enhancing their dispersibility[34] and facilitating covalent interactions with the polymer matrix.[35] Briefly, 100 mg of MWCNTs was refluxed in a mixed acid solution containing concentrated sulfuric acid and nitric acid (3:1 v/v) at 80 °C for 6 h.[36] The resulting suspension was washed repeatedly with ultrapure water until pH become neutral[37] and then dried in a vacuum oven at 60 °C for 24 h. A homogeneous dispersion of MWCNTs was prepared by ultrasonically dispersing 1 mg/mL functionalized MWCNTs in deionized water containing 0.1% SDS for 1 h. Five microliters of the MWCNT dispersion was drop-cast onto the pretreated GCE surface and allowed to dry under an infrared lamp for 30 min.

The MIP film was subsequently synthesized on the MWCNT-modified electrode surface through *in situ* radical polymerization. The pre-polymerization mixture consisted of 0.1 mmol acrylamide (AAM) as the functional monomer, 0.02 mmol MBA as the cross-linker, and 1 mM ephedrine hydrochloride as the template molecule, dissolved in 10 mL of PBS (pH 7.0). After stirring the solution for 30 min to establish pre-polymerization interactions, 0.01 g of APS was added to initiate polymerization. The electrode was immersed in this solution, and polymerization was carried out at room temperature in nitrogen atmosphere for 4 h to prevent oxidative side reactions. After polymerization, the template molecule was removed by immersing the modified electrode in a 10% (v/v) acetic acid solution containing 0.1% SDS and gently stirring for 2 h. The electrodes were then rinsed thoroughly with ultrapure water and dried under nitrogen gas. For comparison, non-imprinted polymer (NIP) electrodes were prepared using the same procedure but omitting the addition of ephedrine hydrochloride in the pre-polymerization mixture. A schematic representation of the overall fabrication procedure is provided in Fig. 1.

2.3 Electrochemical measurements

The electrochemical performance of the fabricated sensors was evaluated using CV, DPV, and EIS in a 5 mM $[Fe(CN)_6]^{3-/4-}$ solution containing 0.1 M KCl. For CV measurements, the potential was swept between –0.2 and +0.6 V at a scan rate of 50 mV/s. DPV measurements were carried out under optimized conditions with a pulse amplitude of 50 mV and a pulse width of 0.05 s.

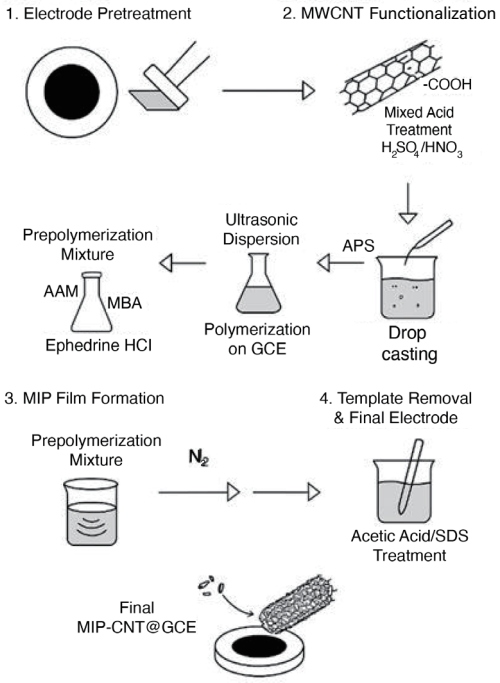

Fig. 1. Fabrication of MIP-CNT composite film-modified electrodes. The process involves electrode pretreatment, the carboxylation of MWCNTs via mixed acid treatment, the drop-casting of functionalized MWCNTs onto the GCE surface, followed by the *in situ* polymerization of the MIP layer in the presence of the template molecule (ephedrine hydrochloride). Finally, template removal using acetic acid/SDS solution yields the selective MIP-CNT@GCE sensor.

Calibration curves for ephedrine detection were established by immersing the MIP-modified electrodes in standard solutions of ephedrine with concentrations ranging from 0.1 to 10 μM. The limit of detection (LOD) was calculated on the basis of a signal-to-noise ratio of 3. Selectivity studies were conducted using structurally related compounds such as pseudoephedrine, norephedrine, and phenylephrine, each at a concentration of 1 μM, to evaluate potential interference.

Stability, repeatability, and reproducibility assessments were conducted by measuring the sensor response over multiple cycles and after storage at 4 °C for up to 14 days. Real sample analysis was performed by spiking urine samples with known concentrations of ephedrine. The samples were diluted 10 times with PBS before analysis, and recovery rates were calculated to evaluate the practical applicability of the sensor.

3. Results and Discussion

3.1 Structural and morphological characterization

The structural and morphological properties of the synthesized MIP-CNT composite films were systematically analyzed to confirm the successful fabrication and functional integration of the composite materials. Comparative evaluations were performed against NIP films and

pristine MWCNTs to elucidate the modifications introduced through the imprinting and composite formation processes.

FTIR was employed to investigate the functional groups present in the MIP-CNT composites and to verify the interactions between the polymer matrix and the incorporated carbon nanotubes.[38] As shown in Fig. 2(a), the spectrum displayed a broad absorption band in the region of 3400–3450 cm^{-1}, corresponding to the O–H and N–H stretching vibrations,[39] indicating the presence of hydroxyl and amine groups from the acrylamide monomer.[40] A distinct peak appeared at 1660 cm^{-1}, corresponding to the C=O stretching vibration of the carboxyl functional groups introduced via the acid treatment of MWCNTs, confirming the effective integration of functionalized CNTs into the MIP matrix.[29] Additionally, a sharp peak at 1558 cm^{-1} observed in the MIP-CNT spectrum was assigned to the C=N stretching of imine bonds, suggesting successful cross-linking between the functional monomer and the CNT framework.[41] Notably, the intensity of the C–N stretching vibration at 1380 cm^{-1} increased significantly in the MIP-CNT sample compared with both MIP and NIP, further corroborating the formation of a robust polymer-CNT hybrid network.[42] The characteristic peaks at 1100 cm^{-1}, attributed to the C–O–C stretching vibration, confirmed the presence of the polymer backbone.[43]

The crystallinity and phase structure of the MIP-CNT were examined by XRD.[44,45] As illustrated in Fig. 2(b), pristine MWCNTs exhibited a strong diffraction peak at 2θ = 26.4°, corresponding to the (002) plane of graphitic carbon, and a secondary peak at 43.2°, associated with the (100) plane.[46] These peaks are indicative of the highly ordered graphitic structure of the MWCNTs.[47] The MIP-CNT sample showed a broad, less intense peak centered at 2θ = 21.8°, characteristic of the amorphous nature of the polymer matrix.[48,49] The (002) diffraction peak of the CNTs was still visible but with reduced intensity, suggesting the partial dispersion of the nanotubes within the polymer matrix[50] and the possible disruption of their long-range order due to polymer coating.[51] This observation confirms the successful embedding of CNTs within the MIP structure without significant aggregation.[52]

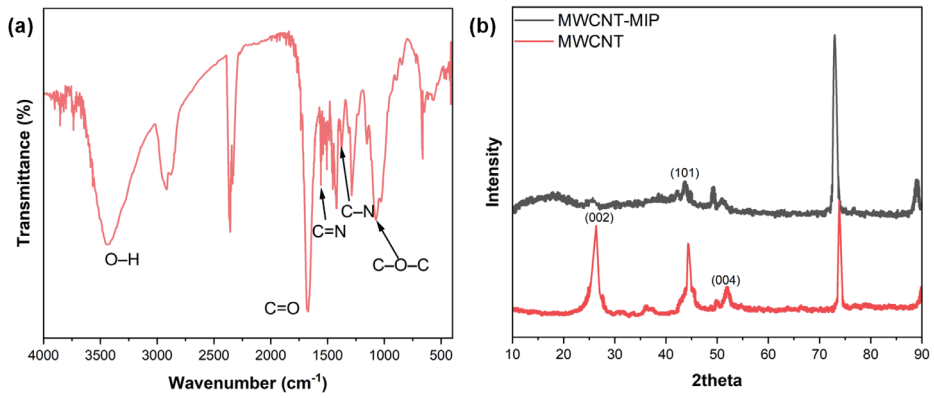

Fig. 2. (Color online) (a) FTIR spectra of MIP-CNT composites, confirming functional group modifications and successful polymer-CNT integration. (b) XRD patterns of pristine CNTs and MIP-CNT composites showing changes in crystallinity after composite formation.

The surface morphologies of the bare GCE, MWCNT-modified GCE, MIP-modified GCE, and MIP-CNT composite-modified GCE were characterized by SEM.[53] As shown in Fig. 3(a), the bare GCE displayed a smooth and featureless surface.[54] After modification with MWCNTs [Fig. 3(b)], a network-like structure consisting of entangled nanotubes was observed,[55] providing a high surface area conducive to polymer deposition.[56] The MIP-modified electrode [Fig. 3(c)] exhibited a homogeneous but dense polymer film with limited porosity, indicating poor mass transport channels for analyte diffusion.[57] In contrast, the MIP-CNT composite film [Fig. 3(d)] presented a porous, interconnected network where CNTs were embedded within the polymer matrix, creating accessible cavities ideal for analyte binding. This morphological configuration is essential for efficient molecular recognition and rapid electron transfer, explaining the superior performance of the MIP-CNT sensors.[58]

TEM was further employed to explore the internal morphology and nanoscale dispersion of CNTs within the polymer matrix.[37] Figure 3(e) shows that in the MIP-CNT composite, the CNTs were uniformly dispersed without significant aggregation and tightly coated by the polymer network. The presence of a thin polymer layer (~10 nm thickness) surrounding the CNTs was evident, which plays a critical role in providing selective molecular recognition while maintaining high electrical conductivity. The tubular structure of the CNTs remained intact after functionalization and polymerization, ensuring effective electron transport throughout the composite material.[59,60] The uniform distribution of polymer-coated CNTs also confirms the efficiency of the *in situ* polymerization approach used in this work.[61]

Elemental mapping analysis using EDS confirmed the spatial distributions of carbon, oxygen, and nitrogen elements across the MIP-CNT composite surface. As shown in Fig. 4, carbon was homogeneously distributed, verifying the presence of the CNT framework.[62,63] The distribution

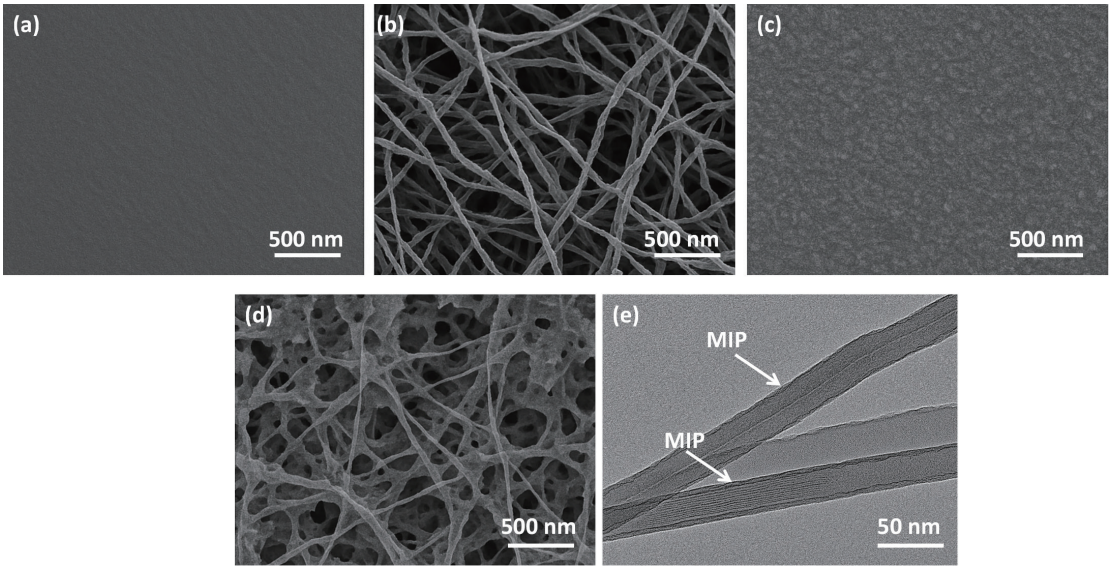

Fig. 3. SEM images of (a) bare GCE, (b) MWCNT-modified GCE, (c) MIP-modified GCE, and (d) MIP-CNT composite film. (e) TEM images illustrating the uniform dispersion of CNTs within the polymer matrix and the formation of thin polymer coatings.

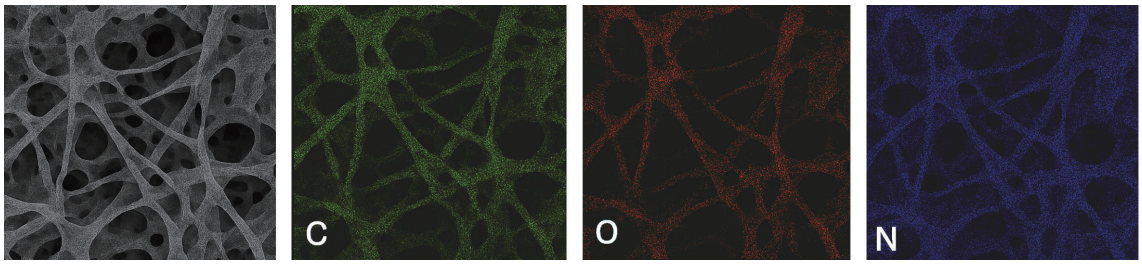

Fig. 4. (Color online) MAP images of carbon, oxygen, and nitrogen distributions across the MIP-CNT composite surface.

of oxygen was slightly enriched around certain regions, corresponding to the carboxyl-functionalized CNTs and polymer carbonyl groups. Nitrogen was uniformly distributed, indicating the successful incorporation of amine functional groups from the polymer network.[64] This uniform elemental distribution supports the successful synthesis of a chemically homogeneous composite material, which is essential for reproducible and selective sensing performance.[65]

XPS was employed to further investigate the surface chemical composition and bonding states of the MIP-CNT composites. The survey spectra [Fig. 5(a)] revealed the presence of prominent peaks corresponding to C 1s, O 1s, and N 1s,[66] confirming the successful incorporation of oxygen- and nitrogen-containing functional groups from the MWCNTs and polymer.[67] High-resolution C 1s spectra [Fig. 5(b)] were deconvoluted into four components: the dominant peak at 284.6 eV assigned to C–C/C=C bonds,[68] a peak at 285.7 eV corresponding C–N bonds,[69,70] a peak at 286.9 eV attributed to C–O bonds, and a peak at 288.4 eV representing O=C–N bonds. The increased intensity of the C–N and O=C–N peaks in the MIP-CNT composite compared with the NIP film directly indicates the formation of imine bonds and cross-linked polymer structures associated with the molecular imprinting process.[71] The N 1s spectrum [Fig. 5(c)] showed peaks at 399.5 and 401.0 eV, corresponding to amine ($–NH_2$) and imine (–C=N) groups, respectively.[72] The presence of these functional groups is critical for the specific binding interactions with ephedrine molecules.

3.2 Electrochemical behavior analysis

Electrochemical characterization is critical for evaluating the electron transfer capabilities, surface reactivity, and molecular recognition behavior of modified electrodes.[73,74] In this study, cyclic voltammetry (CV) and electrochemical impedance spectroscopy (EIS) were employed systematically to investigate the electrochemical properties of the fabricated sensors at various stages of electrode modification.[75] The CV responses of the electrodes during the stepwise modification were recorded in a 5 mM $[Fe(CN)_6]^{3-/4-}$ solution containing 0.1 M KCl at a scan rate of 50 mV/s. As illustrated in Fig. 6(a), the bare GCE exhibited well-defined redox peaks at 0.18 and 0.32 V, corresponding to the reversible redox behavior of the ferri/ferrocyanide couple.[76] The peak-to-peak separation (ΔEp) was calculated to be 140 mV, indicative of a moderately fast electron transfer.[77]

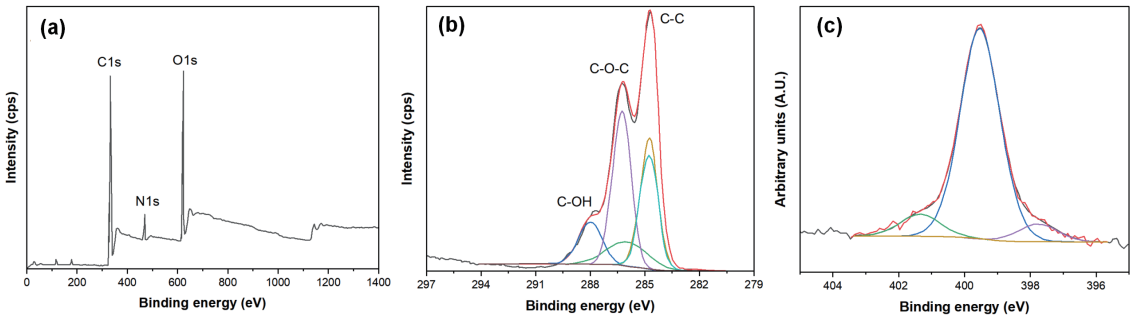

Fig. 5. (Color online) (a) XPS survey spectra showing the elemental composition of the MIP-CNT composite, (b) high-resolution C 1s spectra, and (c) N 1s spectra indicating the chemical states of nitrogen species.

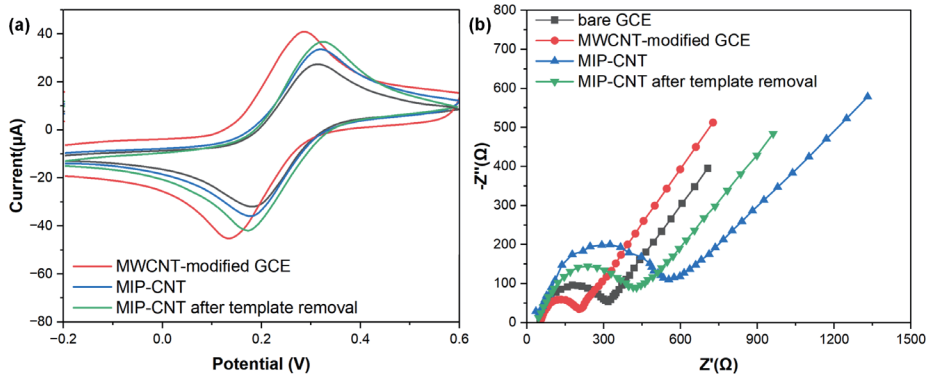

Fig. 6. (Color online) (a) CV and (b) Nyquist plots recorded at various stages of electrode modification in 5 mM $[Fe(CN)_6]^{3-/4-}$ containing 0.1 M KCl: bare GCE, MWCNT-modified GCE, MIP-CNT before template removal, and MIP-CNT after template removal.

Upon modification with functionalized MWCNTs, the redox peak currents significantly increased and ΔEp decreased to 135 mV, suggesting a notable improvement in electron transfer rate due to the high electrical conductivity and surface area provided by the CNT network. When the MIP layer was polymerized onto the MWCNT-modified electrode, the redox peak currents decreased substantially and ΔEp increased to 158 mV. This phenomenon can be attributed to the insulating nature of the polymer film, which partially hinders electron transfer between the redox probe and the electrode surface.(78)

Following template removal, the CV curve of the MIP-CNT-modified electrode showed the partial recovery of the redox peak currents. This improvement is attributed to the formation of recognition cavities within the polymer matrix,(79) which facilitated mass transport(80) and improved the accessibility of the redox probe to the electrode surface.(81) These findings confirm the successful fabrication of the molecularly imprinted polymer with accessible recognition sites.

Electrochemical impedance spectroscopy was conducted to further analyze the interfacial electron transfer resistance at each electrode modification stage. The Nyquist plots obtained in 5 mM $[Fe(CN)_6]^{3-/4-}$ solution are depicted in Fig. 6(b). The bare GCE exhibited a semicircular region at high frequencies, reflecting moderate electron transfer kinetics. After modification

with functionalized MWCNTs, the diameter of the semicircle decreased markedly and Rct was also decreased, indicating a significant improvement in charge transfer at the electrode interface.[82] This observation is consistent with the excellent conductivity of MWCNTs and their role in facilitating fast electron transport.[83–85]

The deposition of the MIP film on the MWCNT-modified electrode caused a substantial increase in peak-peak separation, demonstrating that the insulating polymer matrix restricted electron transfer. However, following the template removal process, Rct decreased, confirming the formation of recognition cavities and the restoration of effective electron pathways. These results collectively validate the successful fabrication of a highly conductive and selectively permeable MIP-CNT composite film, capable of enhancing electron transfer while providing specific molecular recognition functionality for ephedrine.

3.3 Analytical performance of the sensor

The analytical performance of the developed MIP-CNT composite sensor was systematically evaluated to determine its sensitivity, detection limit, linear working range, and overall suitability for practical application in ephedrine detection. These parameters were compared with conventional sensors reported in the literature to assess the technological advantages of the developed system.

DPV was employed to establish the calibration curve for ephedrine detection using the MIP-CNT composite-modified electrode. Measurements were performed in 0.1 M PBS (pH 7.0) under optimized electrochemical parameters. For each concentration, triplicate measurements (n = 3) were performed, and the resulting data are presented in Fig. 7(b) with error bars representing the standard deviation. As shown in Fig. 7, the oxidation peak current decreased linearly with increasing ephedrine concentration over a range of 0.05 to 50 μM, demonstrating excellent reproducibility across repeated measurements (relative standard deviation < 3%).

The regression equation obtained from the calibration plot was expressed as

$$Ip\ (\mu A) = -26.0322 \times \mathrm{Log}_{Cephedrine}\ (\mathrm{nM}) + 223.558\ (R^2 = 0.989).$$

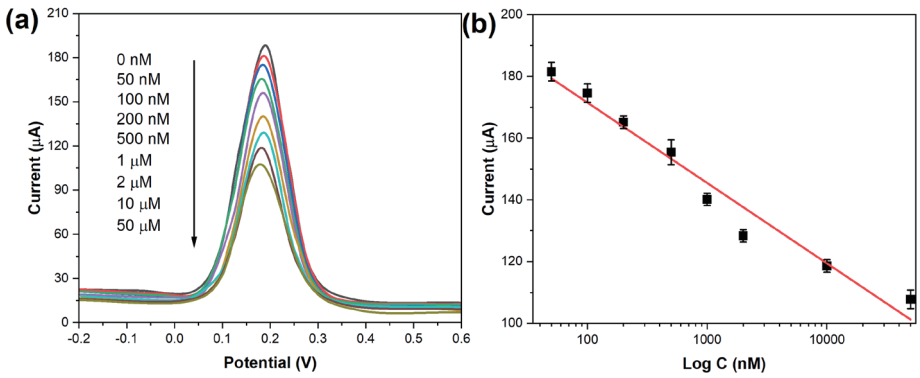

Fig. 7. (Color online) (a) DPV curves and (b) calibration curve for ephedrine detection using the MIP-CNT composite sensor obtained by DPV in 0.1 M PBS (pH 7.0) (*mean* ± *SD*, n = 3). Error bars indicate standard deviation across triplicate measurements

The sensor exhibited excellent linearity (R^2 = 0.998), indicating a strong correlation between the ephedrine concentration and the measured peak current. The LOD calculated on the basis of a signal-to-noise ratio of 3 (S/N = 3) was determined to be 15 nM. The high sensitivity of 26.03 μA/nM reflects the excellent electron transfer capability and effective molecular recognition provided by the MIP-CNT composite.[86,87] This superior performance is attributed to the synergistic effect of the highly conductive CNTs[88] and the selective binding cavities introduced by molecular imprinting.[89]

To further demonstrate the advancement provided by the MIP-CNT composite sensor, its analytical performance was compared with those of previously reported electrochemical sensors for ephedrine detection. It is evident from the comparison that the MIP-CNT composite sensor outperforms conventional electrodes such as unmodified carbon paste electrodes, glassy carbon electrodes modified with metal nanoparticles, and previously reported MIP-based sensors without conductive nanomaterial integration. While prior works reported LOD values ranging from 0.1 to 0.5 μM, the sensor presented in this study achieves an ultralow LOD of 15 nM. Similarly, the sensitivity of the current sensor surpasses the majority of reported values, highlighting its potential for the trace-level detection of ephedrine in complex matrices. A detailed quantitative comparison is provided in Table 1. The developed sensor exhibits the widest linear range (0.05–50 μM), low LOD (15 nM), and high sensitivity (26.03 μA/nM). These results demonstrate the considerable advantage of combining molecular imprinting technology with conductive nanomaterials, which leads to both high selectivity and excellent electron transfer efficiency.

3.4 Selectivity and interference studies

Selectivity is a critical performance parameter for molecularly imprinted sensors, especially when applied to complex sample matrices where structurally similar substances and coexisting species may interfere with target analyte detection. To evaluate the selectivity of the MIP-CNT composite sensor toward ephedrine, DPV measurements were performed in the presence of potential interfering compounds commonly found in biological and pharmaceutical samples.

Figure 8 shows the DPV responses of the MIP-CNT sensor to 10 μM ephedrine and an equimolar concentration of structurally related compounds, including pseudoephedrine, norephedrine, phenylephrine, and dopamine.[94] While all analytes produced detectable current responses, the oxidation peak current corresponding to ephedrine was significantly higher, demonstrating the superior binding affinity of the imprinted cavities for ephedrine molecules.[95]

Table 1
Comparative analysis of the developed MIP-CNT composite sensor with previously reported electrochemical sensors for ephedrine detection.

Sensor type	Linear range (μM)	LOD	Reference
MWCNT/Nafion/MIP/GCE	0.18–75	72 nM	(90)
Fe_3O_4@SiO_2@TiO_2-MIP	0.009–2.8	3.6 nM	(91)
Poly (4-amino−3-hydroxynaphthalene sulfonic acid)/GCE	8–1000	0.78 μM	(92)
C18 bonded silica gel/CPE	2.2–76	—	(93)
MIP-CNT composite (this work)	0.05–50	0.015	This work

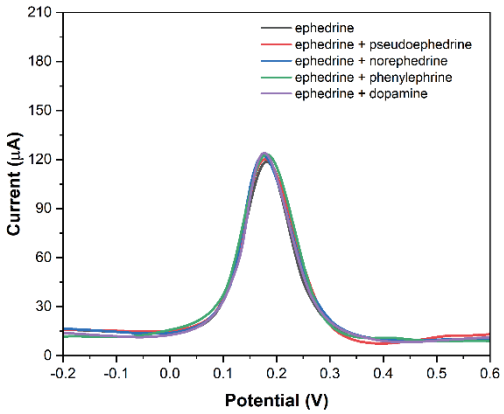

Fig. 8. (Color online) DPV responses of the MIP-CNT composite sensor to ephedrine (10 μM) and common interfering compounds (10 μM each): pseudoephedrine, norephedrine, phenylephrine, and dopamine.

As summarized in Table 2, the highest K value of 5.6 was obtained for pseudoephedrine, indicating that although structurally similar, pseudoephedrine binding was significantly less favored. Lower K values for norephedrine (4.3), phenylephrine (3.1), and dopamine (2.7) further support the high selectivity of the MIP-CNT sensor.[96] These results confirm that the fabricated molecular recognition sites exhibit high shape and functional group complementarity for ephedrine, effectively discriminating against common interfering species.[97]

3.5 Repeatability, reproducibility, and stability

The practical applicability of a sensor relies heavily on its operational repeatability, reproducibility across multiple fabrications, and long-term stability. These factors were systematically evaluated for the developed MIP-CNT composite sensor. The repeatability of the sensor was assessed by five consecutive measurements of 10 μM ephedrine under identical experimental conditions. As shown in Fig. 9(a), the current responses remained highly consistent, with a relative standard deviation (*RSD*) of 2.1%, indicating excellent short-term measurement stability.

To evaluate reproducibility, five independent MIP-CNT-modified electrodes were fabricated using the same preparation protocol, and the current response to 10 μM ephedrine was recorded for each electrode. The *RSD* for these measurements was calculated to be 3.4%, confirming the reproducibility and robustness of the fabrication process.

The long-term stability of the sensor was examined by measuring its response to 10 μM ephedrine after storage at 4 °C for up to 30 days. As shown in Fig. 9(b), the current response retained 95.2% of its initial value after 15 days and 91.3% after 30 days. This minor reduction in response is attributed to the gradual surface fouling and potential partial degradation of the polymer matrix over time. These results demonstrate that the developed sensor maintains high stability over a reasonable storage period, making it suitable for practical deployment in field applications.

Table 2
Selectivity coefficients (*K* values) of the MIP-CNT sensor for ephedrine against common interfering substances.

Interfering compound	Oxidation peak current (μA)	*K* (selectivity)
Ephedrine	18.3	1.0 (reference)
Pseudoephedrine	3.3	5.6
Norephedrine	4.2	4.3
Phenylephrine	5.9	3.1
Dopamine	6.8	2.7

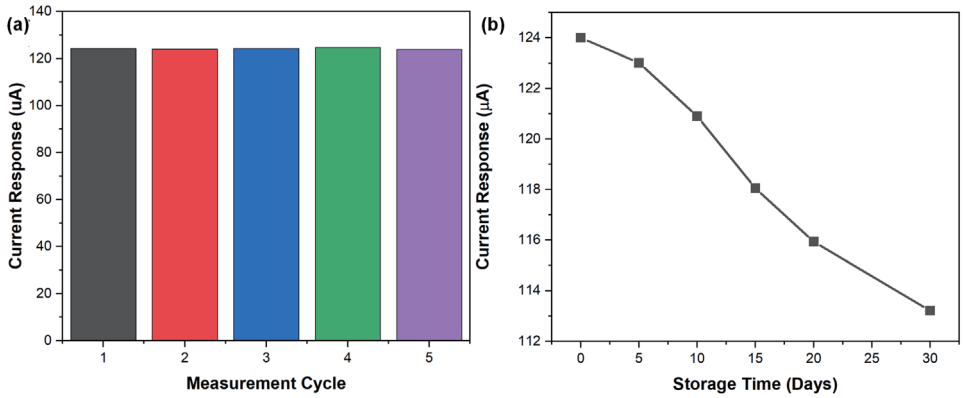

Fig. 9. (Color online) (a) Repeatability study showing consistent DPV responses of the MIP-CNT sensor for five consecutive measurements of 10 μM ephedrine. (b) Long-term stability of the MIP-CNT sensor measured over 30 days at 4 °C.

3.6 Real sample analysis

To verify the practical applicability of the developed MIP-CNT sensor, real sample analysis was conducted using spiked human serum and urine samples. These biological matrices were selected owing to their complex composition and relevance in clinical and forensic drug monitoring. Prior to analysis, the collected serum and urine samples were centrifuged at 4000 rpm for 10 min to remove particulates and diluted tenfold with 0.1 M phosphate-buffered saline (pH 7.0). Known concentrations of ephedrine were then added to the diluted samples to assess recovery performance.

The recovery results summarized in Table 3 indicate that the developed sensor achieved excellent recovery rates ranging from 96.3 to 103.5% in serum samples and from 95.4 to 102.8% in urine samples. The *RSD*s for all measurements were below 4%, indicating high precision and reliability. These recovery values fall well within the acceptable range for bioanalytical method validation, confirming the accuracy and robustness of the sensor in real-world sample testing. These findings highlight the strong potential of the MIP-CNT sensor for application in clinical diagnostics and anti-doping control, where the reliable detection of trace amounts of stimulant drugs in biological fluids is critical.

3.7 Proposed sensing mechanism

The enhanced electrochemical performance of the MIP-CNT sensor can be attributed to the synergistic combination of the molecularly imprinted polymer and the conductive carbon nanotube framework. The proposed sensing mechanism is illustrated schematically in Fig. 10. During fabrication, ephedrine molecules act as the template to form specific recognition sites within the polymer matrix. These cavities exhibit complementary shape, size, and functional group orientation to the target molecule, facilitating selective rebinding during the sensing process. Upon exposure to ephedrine, the molecules diffuse through the porous polymer network and bind specifically to the imprinted cavities. This selective binding process effectively concentrates the analyte near the electrode surface, enhancing the local analyte concentration and facilitating electron transfer.

Simultaneously, the integrated MWCNTs provide highly conductive pathways, accelerating electron transfer from the analyte to the electrode surface. The interconnected nanotube network not only improves conductivity but also offers additional adsorption sites, contributing to signal

Table 3
Recovery results of ephedrine in human serum and urine samples.

Sample type	Added concentration (μM)	Found concentration (μM)	Recovery (%)	*RSD* (%)
Serum	5.0	5.18	103.5	3.2
Serum	10.0	9.75	97.5	2.8
Serum	20.0	19.26	96.3	2.5
Urine	5.0	5.14	102.8	3.5
Urine	10.0	9.85	98.5	3.0
Urine	20.0	19.08	95.4	2.7

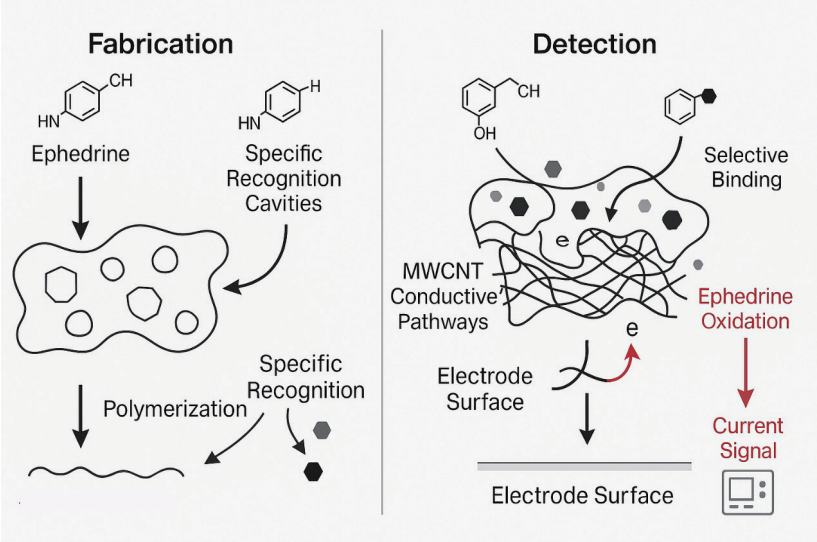

Fig. 10. (Color online) Schematic illustration of the proposed sensing mechanism. Formation of molecularly imprinted cavities specific to ephedrine. Selective binding of ephedrine and facilitated electron transfer through the CNT network during electrochemical detection.

amplification. When a potential is applied, the bound ephedrine molecules undergo oxidation at the electrode surface, resulting in a measurable current response. The combination of selective molecular recognition and efficient charge transport leads to high sensitivity and low detection limits, even in the presence of structurally similar interfering substances. This dual-functional mechanism ensures both the selectivity provided by the MIP layer and the signal enhancement offered by the CNT framework, making the sensor highly effective for real-world analytical applications.

4. Conclusions

We successfully engineered and rigorously evaluated a novel electrochemical sensor for ephedrine detection, leveraging a MIP-CNT composite film on a GCE. Comprehensive characterization using FTIR, XRD, SEM, TEM, MAP, and XPS confirmed the effective synthesis and synergistic integration of the MIP and CNT components, highlighting a porous, interconnected network with uniformly dispersed CNTs coated by a polymer layer approximately 10 nm thick, which facilitated enhanced analyte interaction and signal transduction. Electrochemical analyses via CV and EIS demonstrated improved electron transfer kinetics, with the ΔEp for the redox probe decreasing to 135 mV on the MWCNT-modified GCE from 140 mV on the bare GCE, and successful template removal was evidenced by favorable changes in redox currents and Rct. The developed MIP-CNT sensor exhibited outstanding analytical performance for ephedrine, achieving a wide linear detection range from 0.05 to 50 μM, an ultralow LOD of 15 nM, and a high sensitivity of 26.03 μA/nM. Crucially, the sensor demonstrated excellent selectivity against common interfering substances such as pseudoephedrine (selectivity coefficient K = 5.6), norephedrine (K = 4.3), phenylephrine (K = 3.1), and dopamine (K = 2.7). The sensor also showed marked operational characteristics, with *RSD*s of 2.1% for repeatability and 3.4% for reproducibility. Furthermore, it maintained 91.3% of its initial response after 30 days of storage at 4 °C. Real sample analysis in spiked human serum and urine yielded excellent recovery rates, ranging from 95.4 to 103.5% with *RSD*s below 4%, underscoring its practical applicability. These results collectively affirm that the synergistic combination of MIPs' molecular recognition capabilities with CNTs' superior electrical properties provides a robust and highly effective platform for the sensitive and selective determination of ephedrine in complex biological samples.

References

1 N. Felipe Montiel, M. Parrilla, N. Sleegers, F. Van Durme, A. L. N. Van Nuijs, and K. De Wael: SSRN Electron. J. (2022). https://doi.org/10.2139/ssrn.4219018
2 H.-J. Yoo, H.-Y. Yoon, J. Yee, and H.-S. Gwak: Pharmaceuticals **14** (2021) 1198. https://doi.org/10.3390/ph14111198
3 D. D. Umashankar: J. Phytopharm. **9** (2020) 270. https://doi.org/10.31254/phyto.2020.9410
4 Anesthesiology **134** (2021) 420. https://doi.org/10.1097/ALN.0000000000003707
5 Y.-E. Kang, J. Chae, T. T. Nguyen, J.-J. Kang, and S.-Y. Oh: Neuro-ophthalmol. **48** (2024) 193. https://doi.org/10.1080/01658107.2023.2301363
6 M. Protti, R. Mandrioli, J. Gonzalez-Rodriguez, and L. Mercolini: J. Chromatogr. Open **2** (2022) 100032. https://doi.org/10.1016/j.jcoa.2022.100032

7 A. Mobed, M. Darvishi, A. Tahavvori, I. Alipourfard, F. Kohansal, F. Ghazi, and V. Alivirdiloo: J. Clin. Lab. Anal. **38** (2024) e25006. https://doi.org/10.1002/jcla.25006
8 L. Collins, E. Angley, J. Smith, F. Cameron, and P. Stewart: J. Paediatr. Child Health **60** (2024) 610. https://doi.org/10.1111/jpc.16649
9 X. Xuan, C. Pérez-Ràfols, C. Chen, M. Cuartero, and G. A. Crespo: ACS Sens. **6** (2021) 2763. https://doi.org/10.1021/acssensors.1c01009
10 S. Fuchs, S. Johansson, A. Ø. Tjell, G. Werr, T. Mayr, and M. Tenje: ACS Biomater. Sci. Eng. **7** (2021) 2926. https://doi.org/10.1021/acsbiomaterials.0c01110
11 V. Reyes-Loaiza, J. De La Roche, E. Hernandez-Renjifo, O. Idárraga, M. Da Silva, D. P. Valencia, T. Ghneim-Herrera, and A. Jaramillo-Botero: Sci. Rep. **14** (2024) 5772. https://doi.org/10.1038/s41598-024-56212-0
12 S. E. Elugoke, A. S. Adekunle, O. E. Fayemi, E. D. Akpan, B. B. Mamba, E. M. Sherif, and E. E. Ebenso: Electrochem. Sci. Adv. **1** (2021) e2000026. https://doi.org/10.1002/elsa.202000026
13 L. Wang, M. Pagett, and W. Zhang: Sens. Actuators Rep. **5** (2023) 100153. https://doi.org/10.1016/j.snr.2023.100153
14 E. N. Ndunda: J. Mol. Recognit. **33** (2020) e2855. https://doi.org/10.1002/jmr.2855
15 S. Wang, R. Shao, W. Li, X. Li, J. Sun, S. Jiao, S. Dai, M. Dou, R. Xu, Q. Li, and J. Li: ACS Appl. Mater. Interfaces **14** (2022) 18845. https://doi.org/10.1021/acsami.2c01014
16 W. Li, S. Xu, Y. Li, J. Chen, Y. Ma, and Z. Liu: CCS Chem. **5** (2023) 497. https://doi.org/10.31635/ccschem.022.202101747
17 S. N. Samanci, A. Cetinkaya, N. Doufene, N. Bounoua, S. I. Kaya, E. B. Atici, and S. A. Ozkan: J. Electrochem. Soc. **171** (2024) 37504. https://doi.org/10.1149/1945-7111/ad2cba
18 D. Feng, J. Dai, Y. Yan, and C. Li: Catalysts **15** (2025) 192. https://doi.org/10.3390/catal15020192
19 T. Lai, H. Shu, B. Yao, S. Lai, T. Chen, X. Xiao, and Y. Wang: Biosensors **13** (2023) 505. https://doi.org/10.3390/bios13050505
20 R. Apak, A. Üzer, Ş. Sağlam, and A. Arman: Electroanalysis **35** (2023) e202200175. https://doi.org/10.1002/elan.202200175
21 C. Laghlimi, A. Moutcine, A. Chtaini, J. Isaad, A. Soufi, Y. Ziat, H. Amhamdi, and H. Belkhanchi: ADMET DMPK (2023). https://doi.org/10.5599/admet.1709
22 L. Najmi and Z. Hu: J. Compos. Sci. **7** (2023) 165. https://doi.org/10.3390/jcs7040165
23 A. R. Selvaraj, A. Muthusamy, Inho-Cho, H.-J. Kim, K. Senthil, and K. Prabakar: Carbon **174** (2021) 463. https://doi.org/10.1016/j.carbon.2020.12.052
24 W. Shehzad, M. R. A. Karim, M. Z. Iqbal, N. Shahzad, and A. Ali: J. Energy Storage **54** (2022) 105231. https://doi.org/10.1016/j.est.2022.105231
25 Q. Chen, Y.-Y. Zhang, P. Huang, Y.-Q. Li, and S.-Y. Fu: Compos. Commun. **30** (2022) 101083. https://doi.org/10.1016/j.coco.2022.101083
26 Y.-J. Wan, X.-Y. Wang, X.-M. Li, S.-Y. Liao, Z.-Q. Lin, Y.-G. Hu, T. Zhao, X.-L. Zeng, C.-H. Li, S.-H. Yu, P.-L. Zhu, R. Sun, and C.-P. Wong: ACS Nano **14** (2020) 14134. https://doi.org/10.1021/acsnano.0c06971
27 Y.-X. Wang, M. Rinawati, J.-D. Zhan, K.-Y. Lin, C.-J. Huang, K.-J. Chen, H. Mizuguchi, J.-C. Jiang, B.-J. Hwang, and M.-H. Yeh: ACS Appl. Nano Mater. **5** (2022) 11100. https://doi.org/10.1021/acsanm.2c02279
28 X. Li, Y. Li, P. Yu, Y. Tong, and B.-C. Ye: Analyst **146** (2021) 6323. https://doi.org/10.1039/D1AN01413G
29 G. S. Geleta: Sens. Bio-Sens. Res. **43** (2024) 100610. https://doi.org/10.1016/j.sbsr.2023.100610
30 S. Wjihi, F. Aouaini, A. H. Almuqrin, and A. B. Lamine: Arabian J. Chem. **13** (2020) 6876. https://doi.org/10.1016/j.arabjc.2020.06.040
31 K. Vispute, A. Mukke, and A. P. More: Polym. Adv. Technol. **35** (2024) e6218. https://doi.org/10.1002/pat.6218
32 I.-A. Pavel, S. Lakard, and B. Lakard: Chemosensors **10** (2022) 97. https://doi.org/10.3390/chemosensors10030097
33 T. Zhu, Y. Ni, G. M. Biesold, Y. Cheng, M. Ge, H. Li, J. Huang, Z. Lin, and Y. Lai: Chem. Soc. Rev. **52** (2023) 473. https://doi.org/10.1039/D2CS00173J
34 V. Patel, U. Joshi, A. Joshi, A. D. Oza, C. Prakash, E. Linul, R. D. S. G. Campilho, S. Kumar, and K. K. Saxena: Materials **15** (2022) 7263. https://doi.org/10.3390/ma15207263
35 D.-Y. Kim and S.-H. Park: Korean J. Met. Mater. **60** (2022) 237. https://doi.org/10.3365/KJMM.2022.60.3.237
36 J. Xie, J. Chen, W. Zhou, and Z. Guo: In Review (2023). https://doi.org/10.21203/rs.3.rs-3321663/v1
37 Z. Shang, B. Song, H. Li, H. Zhang, F. Feng, J. Kaelin, W. Zhang, B. Xie, Y. Cheng, K. Lu, and Q. Chen: CCS Chem. **4** (2022) 2115. https://doi.org/10.31635/ccschem.021.202101106
38 O. Gupta, S. Roy, L. Rao, and S. Mitra: Membranes **12** (2022) 1227. https://doi.org/10.3390/membranes12121227
39 M. Hao, Z. Chen, X. Liu, X. Liu, J. Zhang, H. Yang, G. I. N. Waterhouse, X. Wang, and S. Ma: CCS Chem. **4** (2022) 2294. https://doi.org/10.31635/ccschem.022.202201897

40 X. Zhang, J. You, J. Zhang, C. Yin, Y. Wang, R. Li, and J. Zhang: CCS Chem. **5** (2023) 2140. https://doi.org/10.31635/ccschem.022.202202388
41 C. Ji, K. Su, W. Wang, J. Chang, E.-S. M. El-Sayed, L. Zhang, and D. Yuan: CCS Chem. **4** (2022) 3095. https://doi.org/10.31635/ccschem.021.202101453
42 S. S. Mane and G. M. Joshi: J. Appl. Polym. Sci. **141** (2024) e55249. https://doi.org/10.1002/app.55249
43 Y. Li, Z. Zhang, X. Han, T. Li, and Y. Lin: CCS Chem. **4** (2022) 1087. https://doi.org/10.31635/ccschem.021.202100832
44 L. Ayyasamy, A. Mohan, L. Rex, V. Sivakumar, S. Dhanasingh, and P. Sivasamy: Therm. Sci. **26** (2022) 1615. https://doi.org/10.2298/TSCI210930019L
45 N. A. M. Razali, R. Mohd Sohaimi, R. N. I. R. Othman, N. Abdullah, S. Z. N. Demon, L. Jasmani, W. M. Z. W. Yunus, W. M. H. W. Ya'acob, E. M. Salleh, M. N. Norizan, and N. A. Halim: Polymers **14** (2022) 387. https://doi.org/10.3390/polym14030387
46 R. Mahato, Sk. Masiul Islam, R. K. Maurya, S. Kumar, G. Purohit, and S. Singh: Phys. Chem. Chem. Phys. **26** (2024) 95. https://doi.org/10.1039/D3CP04158A
47 T. Haldar, U. Kumar, B. C. Yadav, and V. V. R. K. Kumar: J. Appl. Phys. **130** (2021) 75106. https://doi.org/10.1063/5.0049232
48 S. B. Aziz, I. Brevik, M. H. Hamsan, M. A. Brza, M. M. Nofal, A. M. Abdullah, S. Rostam, S. Al-Zangana, S. K. Muzakir, and M. F. Z. Kadir: Polymers **12** (2020) 2257. https://doi.org/10.3390/polym12102257
49 S. N. Hosseini, S. Pirsa, and J. Farzi: Polym. Test. **97** (2021) 107182. https://doi.org/10.1016/j.polymertesting.2021.107182
50 M. A. Saleh and M. K. Jawad: Nano Hybrids Compos. **35** (2022) 85. https://doi.org/10.4028/p-5ijt59
51 J. Xie, J. Li, X. Li, H. Lei, W. Zhuo, X. Li, G. Hong, K. N. Hui, L. Pan, and W. Mai: CCS Chem. **3** (2021) 791. https://doi.org/10.31635/ccschem.020.202000203
52 D. Das, S. Nag, A. Adaval, A. K. Hazarika, S. Sabhapondit, A. R. Bhattacharyya, B. Tudu, R. Bandopadhyay, and R. Banerjee Roy: IEEE Sensors J. **22** (2022) 10323. https://doi.org/10.1109/JSEN.2022.3169169
53 A. Esokkiya, S. Sudalaimani, K. Sanjeev Kumar, P. Sampathkumar, C. Suresh, and K. Giribabu: ACS Omega **6** (2021) 9528. https://doi.org/10.1021/acsomega.0c06315
54 Y. Shao, Y. Zhu, R. Zheng, P. Wang, Z. Zhao, and J. An: Adv. Compos. Hybrid Mater. **5** (2022) 3104. https://doi.org/10.1007/s42114-022-00562-8
55 Q. Li and H. Chen: Int. J. Electrochem. Sci. **18** (2023) 100206. https://doi.org/10.1016/j.ijoes.2023.100206
56 D. Wang, J. Chen, Y. Li, and S. Feng: Small Methods **9** (2025) 2401491. https://doi.org/10.1002/smtd.202401491
57 S. Ahmed, A. Ansari, A. S. Haidyrah, A. A. Chaudhary, M. Imran, and A. Khan: ACS Appl. Polym. Mater. **4** (2022) 2783. https://doi.org/10.1021/acsapm.2c00072
58 X. Zhou, P. Ye, Z. Huang, C. Yang, J. Ren, J. Wang, and S. Tang: Chemosensors **12** (2024) 121. https://doi.org/10.3390/chemosensors12070121
59 Z. Li, D. K. Tran, M. Nguyen, T. Jian, F. Yan, S. A. Jenekhe, and C. Chen: Macromol. Rapid Commun. **43** (2022) 2100639. https://doi.org/10.1002/marc.202100639
60 N. Song, S. Ren, Y. Zhang, C. Wang, and X. Lu: Adv. Funct. Mater. **32** (2022) 2204751. https://doi.org/10.1002/adfm.202204751
61 C. A. C. Chazot, B. Damirchi, B. Lee, A. C. T. Van Duin, and A. J. Hart: Nano Lett. **22** (2022) 998. https://doi.org/10.1021/acs.nanolett.1c03866
62 C. Yuan, P. Zeng, C. Cheng, T. Yan, G. Liu, W. Wang, J. Hu, X. Li, J. Zhu, and L. Zhang: CCS Chem. **4** (2022) 2829. https://doi.org/10.31635/ccschem.021.202101214
63 L. Zhang, T. Wang, T.-N. Gao, H. Xiong, R. Zhang, Z. Liu, S. Song, S. Dai, and Z.-A. Qiao: CCS Chem. **3** (2021) 870. https://doi.org/10.31635/ccschem.020.202000233
64 R.-J. Wei, H.-G. Zhou, Z.-Y. Zhang, G.-H. Ning, and D. Li: CCS Chem. **3** (2021) 2045. https://doi.org/10.31635/ccschem.020.202000401
65 D. Chu, W. Gong, H. Jiang, X. Tang, Y. Cui, and Y. Liu: CCS Chem. **4** (2022) 1180. https://doi.org/10.31635/ccschem.021.202100847
66 Z. Zhou, L. Zhao, Y. Liu, D. Li, Q. Xia, J. Wang, Z. Zhang, X. Han, Y. Long, Y. Zhang, Y. Li, and S. Chou: Renewables **1** (2023) 100. https://doi.org/10.31635/renewables.022.202200004
67 Y. Huang, C. Wang, Y. Yu, Y. Yu, W. Wang, and B. Zhang: CCS Chem. **4** (2022) 1208. https://doi.org/10.31635/ccschem.021.202100809
68 G. Greczynski and L. Hultman: Sci. Rep. **11** (2021) 11195. https://doi.org/10.1038/s41598-021-90780-9
69 Z. Liu, J. Cheng, O. Höfft, and F. Endres: Metals **12** (2021) 59. https://doi.org/10.3390/met12010059
70 Y. Liu, Y. Gao, F. He, Y. Xue, and Y. Li: CCS Chem. **5** (2023) 971. https://doi.org/10.31635/ccschem.022.202202005

71 Y. Wang, K. Yang, J. Wang, H. Yu, J. Cui, and Y. Xiong: Solvent Extr. Ion Exch. **39** (2021) 622. https://doi.org/10.1080/07366299.2021.1876985
72 N. Li, D.-H. Si, Q. Wu, Q. Wu, Y.-B. Huang, and R. Cao: CCS Chem. **5** (2023) 1130. https://doi.org/10.31635/ccschem.022.202201943
73 H. Li, S. Han, X. Niu, and K. Wang: ACS Appl. Mater. Interfaces **15** (2023) 44127. https://doi.org/10.1021/acsami.3c10543
74 L. Wang, W. Gao, S. Ng, and M. Pumera: Anal. Chem. **93** (2021) 5277. https://doi.org/10.1021/acs.analchem.1c00322
75 B. A. Braz, M. Hospinal-Santiani, G. Martins, C. S. Pinto, A. J. G. Zarbin, B. C. B. Beirão, V. Thomaz-Soccol, M. F. Bergamini, L. H. Marcolino-Junior, and C. R. Soccol: Biosensors **12** (2022) 885. https://doi.org/10.3390/bios12100885
76 G. Tesfaye, M. Tessema, and N. Negash: J. Electrochem. Sci. Eng. **13** (2023) 297. https://doi.org/10.5599/jese.1674
77 A. I. Ibrahim and M. M. Radhi: J. Phys. Conf. Ser. **1853** (2021) 12008. https://doi.org/10.1088/1742-6596/1853/1/012008
78 J. Wang, W. Ma, H. Wang, Z. Xie, H. Zhang, and Y. Ma: CCS Chem. **4** (2022) 1347. https://doi.org/10.31635/ccschem.021.202101021
79 Y. Zhou, A. Liu, Y. Li, and S. Liu: Coatings **13** (2023) 1374. https://doi.org/10.3390/coatings13081374
80 L. Deng, J. Liu, H. Huang, C. Deng, L. Lu, L. Wang, and X. Wang: Molecules **28** (2023) 7475. https://doi.org/10.3390/molecules28227475
81 W. Tang, L. Yin, J. R. Sempionatto, J. Moon, H. Teymourian, and J. Wang: Adv. Mater. **33** (2021) 2008465. https://doi.org/10.1002/adma.202008465
82 R. Attias, B. Dlugatch, M. S. Chae, Y. Goffer, and D. Aurbach: Electrochem. Commun. **124** (2021) 106952. https://doi.org/10.1016/j.elecom.2021.106952
83 T. Chang, C. Chuang, Y. Chen, Y. Wang, Y. Gu, and C. Kung: ChemCatChem **14** (2022) e202200199. https://doi.org/10.1002/cctc.202200199
84 G. Zhu, N. Hu, M. Guo, Y. Liu, Q. Ran, and H. Zhao: Mater. Res. Innovations **26** (2022) 389. https://doi.org/10.1080/14328917.2022.2059233
85 S. Zhang, M. Massetti, T. Ruoko, D. Tu, C. Yang, X. Liu, Z. Wu, Y. Lee, R. Kroon, P. O. Å. Persson, H. Y. Woo, M. Berggren, C. Müller, M. Fahlman, and S. Fabiano: Adv. Funct. Mater. **32** (2022) 2106447. https://doi.org/10.1002/adfm.202106447
86 P. Faradilla, H. Setiyanto, R. V. Manurung, and V. Saraswaty: RSC Adv. **12** (2022) 743. https://doi.org/10.1039/D1RA06862H
87 H. H. Shanaah, Z. Ameen, K. Jaafar, A. Hefnawy, H. S. M. Abd-Rabboh, and A. H. Kamel: ChemElectroChem **10** (2023) e202300153. https://doi.org/10.1002/celc.202300153
88 M. Chen, R. Abazari, S. Sanati, J. Chen, M. Sun, C. Bai, A. M. Kirillov, Y. Zhou, and G. Hu: Carbon Energy **5** (2023) e459. https://doi.org/10.1002/cey2.459
89 P. Lach, A. Garcia-Cruz, F. Canfarotta, A. Groves, J. Kalecki, D. Korol, P. Borowicz, K. Nikiforow, M. Cieplak, W. Kutner, S. A. Piletsky, and P. S. Sharma: Biosens. Bioelectron. **236** (2023) 115381. https://doi.org/10.1016/j.bios.2023.115381
90 L. Jia, Y. Mao, S. Zhang, H. Li, M. Qian, D. Liu, and B. Qi: Microchem. J. **164** (2021) 105981. https://doi.org/10.1016/j.microc.2021.105981
91 H. Bagheri, N. Pajooheshpour, A. Afkhami, and H. Khoshsafar: RSC Adv. **6** (2016) 51135. https://doi.org/10.1039/C6RA09488K
92 M. Amare, W. Lakew, and S. Admassie: Anal. Bioanal. Electrochem. **3** (2011) 365.
93 M. Chicharro, A. Zapardiel, L. E. Bermejo, J. Perez, and L. Hernandez: Anal. Lett. **27** (1994) 1809.
94 S. Hong, L. Y. S. Lee, M. So, and K. Wong: Electroanalysis **25** (2013) 1085. https://doi.org/10.1002/elan.201200631
95 S. A. Piletsky, K. Karim, E. V. Piletska, A. P. F. Turner, C. J. Day, K. W. Freebairn, and C. Legge: Analyst **126** (2001) 1826. https://doi.org/10.1039/b102426b
96 J. Li, J. Zhao, and X. Wei: Sens. Actuators, B **140** (2009) 663. https://doi.org/10.1016/j.snb.2009.04.067
97 J.-Y. Zhang, J. Ding, L.-M. Liu, R. Wu, L. Ding, J.-Q. Jiang, J.-W. Pang, Y. Li, N.-Q. Ren, and S.-S. Yang: Environ. Sci. Ecotechnol. **17** (2024) 100308. https://doi.org/10.1016/j.ese.2023.100308